Near ultraviolet photochemistry of 2-bromo- and 2-iodothiophene: Revealing photoinduced ring opening in the gas phase?

Barbara Marchetti, Tolga N. V. Karsili, Orla Kelly, Panos Kapetanopoulos, and Michael N. R. Ashfold

Citation: The Journal of Chemical Physics **142**, 224303 (2015); doi: 10.1063/1.4921315
View online: http://dx.doi.org/10.1063/1.4921315
View Table of Contents: http://scitation.aip.org/content/aip/journal/jcp/142/22?ver=pdfcov
Published by the AIP Publishing

Near ultraviolet photochemistry of 2-bromo- and 2-iodothiophene: Revealing photoinduced ring opening in the gas phase?

Barbara Marchetti,[1] Tolga N. V. Karsili,[1] Orla Kelly,[2] Panos Kapetanopoulos,[2] and Michael N. R. Ashfold[1,a)]
[1]*School of Chemistry, University of Bristol, Cantock's Close, Bristol BS8 1TS, United Kingdom*
[2]*Photek Ltd., 26 Castleham Road, St. Leonards-on-Sea, East Sussex TN38 9NS, United Kingdom*

(Received 24 March 2015; accepted 7 May 2015; published online 9 June 2015)

Velocity map imaging methods, with a new and improved ion optics design, have been used to explore the near ultraviolet photodissociation dynamics of gas phase 2-bromo- and 2-iodothiophene molecules. In both cases, the ground (X) and spin-orbit excited (X*) (where X = Br, I) atom products formed at the longest excitation wavelengths are found to recoil with fast, anisotropic velocity distributions, consistent with prompt C–X bond fission following excitation via a transition whose dipole moment is aligned parallel to the breaking bond. Upon tuning to shorter wavelengths, this fast component fades and is progressively replaced by a slower, isotropic recoil distribution. Complementary electronic structure calculations provide a plausible explanation for this switch in fragmentation behaviour—namely, the opening of a rival C–S bond extension pathway to a region of conical intersection with the ground state potential energy surface. The resulting ground state molecules are formed with more than sufficient internal energy to sample the configuration space associated with several parent isomers and to dissociate to yield X atom products in tandem with both cyclic and ring-opened partner fragments. [http://dx.doi.org/10.1063/1.4921315]

I. INTRODUCTION

Near ultraviolet (UV) photoexcitation of an isolated gas phase molecule at energies above its lowest dissociation limit often results in bond fission. This may occur following radiationless transfer to the ground state potential energy surface (PES) and appropriate intramolecular vibrational redistribution (IVR), or may occur on an excited state PES that is repulsive in the relevant bond coordinate. Excited state dissociations can be viewed in two classes: the dissociative state may be populated directly in the photoexcitation process, or indirectly, following radiationless transfer from an optically "bright" state reached in the initial absorption event. In both cases, there is growing recognition that the excited state PES on which the eventual bond extension occurs is likely to arise as a result of electron promotion to a σ* orbital (i.e., to an orbital that is antibonding in the coordinate of interest).[1,2] This growing recognition accounts for the frequent reference in the recent literature to $n\sigma^*$ and/or $\pi\sigma^*$ excited states, i.e., dissociative excited states formed by electron promotion from an occupied non-bonding (n) or bonding (π) orbital to a σ* orbital.

The present study employs nanosecond pulsed laser pump (photolysis)–probe (resonance enhanced multiphoton ionisation (REMPI)) velocity map imaging (VMI) methods to investigate the bromine and iodine atoms formed following excitation of 2-bromo- and 2-iodothiophene molecules in the gas phase at many near UV wavelengths. The experiments exploit a new ion optics assembly that offers superior velocity mapping (and slicing) capabilities to that we have used previously. Aspects of the design, implementation, and evaluation of this ion optics assembly are presented in Sec. II and, in more detail, in the supplementary material.[3]

Analogy with previous experimental studies of bare and substituted halobenzenes[4–8] encourages the expectation that near UV excitation of the title halothiophenes should result in eventual CX (X = Br, I) bond fission on one or more $(n/\pi)\sigma^*$ excited state PESs. A previous one colour ion imaging study of Br atoms resulting from 267 nm photolysis of 2-bromothiophene lends support to this expectation,[9] as do evident similarities in the resonance Raman (RR) spectra measured following excitation of 2-iodothiophene and iodobenzene (in cyclohexane solution).[10] However, the observation of nominal antisymmetric C–S–C stretching vibrations in the RR spectra of 2-iodothiophene[10] (and of bare thiophene[11]) hints at some contribution from an alternative C–S bond extension (ring-opening) pathway. This finding served to reinforce speculations offered to account for various of the products observed in earlier experimental studies of thiophene photolysis under both bulk[12] and molecular beam[13,14] conditions and accords with conclusions from several recent theoretical studies of the ultrafast deactivation of gas phase thiophene molecules.[15–18]

Finding direct evidence for the operation of such pathways experimentally is a challenge, as any primary ring-opened products will almost inevitably be formed with sufficiently high levels of vibrational excitation to defy

a)Author to whom correspondence should be addressed. Electronic mail: mike.ashfold@bristol.ac.uk. Tel.: +44 (0)117 928 8312.

definitive spectroscopic characterisation and, in many cases, will decay further to smaller secondary products. One way of circumventing these difficulties is to study such photo-induced ring-opening reactions in a weakly interacting solvent, as illustrated by our recent ultrafast pump–(broadband infrared (IR) absorption) probe studies of the 267 nm photolysis of thiophenone in solution in acetonitrile.[19] The additional C=O group (cf. bare thiophene) in this system was crucial, serving as the "messenger" that allowed us to track the photo-induced evolution from parent (the photoexcitation of which results in a characteristic carbonyl stretch bleach feature at ~1650 cm^{-1}) to product (which shows a ketene asymmetric stretch band that narrows and blue shifts to an asymptotic wavenumber of ~2250 cm^{-1} with increasing pump-probe time delays). The time dependence of the ketene absorption reflects the formation, rearrangement, and subsequent vibrational relaxation of the ring-opened product through interaction with the solvent. Such vibrational quenching is, of course, not available in the analogous gas-phase study.

Here, we show that the X atoms in the title halothiophenes can also serve as messengers and, from the wavelength dependence of the X atom product velocities (as revealed by ion imaging), provide clear evidence for photo-induced ring expansion at shorter UV excitation wavelengths. Complementary electronic structure calculations serve to reinforce this interpretation and to highlight the key role of a $(n/\pi)\sigma^*$ PES in driving the C–S bond extension required to access a region of conical intersection (CI) with, and promote radiationless transfer to, the ground state PES and (potentially) to fully ring opened products. This work adds to the growing literature highlighting the importance of $(n/\pi)\sigma^*$ excited states in facilitating both emergent and complete ring opening in heterocyclic molecules.[20–24]

II. EXPERIMENTAL

2-Bromo- and 2-iodothiophene (purity ~98%) were obtained from Sigma Aldrich and used as supplied. The individual samples (both liquids at room temperature) were packed in a stainless steel inline filter positioned upstream of a pulsed valve, which was resistively heated (to ~30 °C) to boost its vapour pressure. This vapour pressure was seeded in helium (at stagnation pressures ~600 and ~400 millibars, respectively) and expanded though the pulsed valve (General Valve, Series No. 9; Parker) into the VMI spectrometer in the form of a skimmed, pulsed molecular beam. The vacuum chamber has been detailed previously, as have the Nd-YAG pumped, frequency doubled, pulsed dye lasers used to generate the requisite photolysis and 2 + 1 REMPI probe wavelengths.[25] The probe wavelengths used in the two colour studies reported here were 266.63 nm and 266.70 nm for ground and spin-orbit (SO) excited Br atoms[26] (henceforth written simply as Br and Br^*) and 303.68 nm and 304.02 nm for I and I^* atoms.[27] All reported images recorded at wavelengths $\lambda > 250$ nm are from "one-colour" experiments, where the same wavelength is used both to effect photodissociation and probe the resulting halogen atom products, whereas those recorded at $\lambda < 250$ nm are from traditional "two-colour" experiments wherein the two pulses are arranged to counter-propagate through the interaction region with a time delay δt ~ 20-45 ns between the photolysis and REMPI laser pulses. The probe laser bandwidth is greater than the Br/I atom Doppler width in all cases and thus was simply fixed at the line centre of the respective transition.

Ions formed in the interaction region were accelerated with a new, purpose designed ion optics assembly detailed below and in the supplementary material,[3] through a field free time-of-flight (TOF) region towards a position sensitive detector (double microchannel plates (MCPs)) coupled to a phosphor screen and a CCD camera (Allied Vision Technologies, Model GC1385). The images were acquired and processed using event counting (LaVision, Davis 6.2) and could be collected as traditional "pancaked" images or, by appropriate adjustment of the electrode voltages, by time gating the front MCP (Photek, GM-MCP-2) so as to take a central slice out of the extended ion cloud of interest at the detector. The pancaked images were transformed and analysed as described previously.[28] The trigger pulses for the pulsed valve, the flashlamps and Q-switches of both Nd-YAG lasers, the gating of the front MCP, and the camera were supplied by a BNC Model 555 delay generator operating under Labview control.

A. The new ion optics assembly

The ion optics assembly developed in this work was designed, built, and assembled following extensive SIMION (v 8.1)[29] simulations. As with several other reported spectrometer designs,[30–36] the ion optics assembly described in Ref. 25 provided a convenient starting point. The result of this analysis is the four electrode stack shown in Fig. 1, which is designed to support a linear mapping of image radius (r) to ion velocity (v) right down to $r = 0$, a larger interaction volume capable of supporting optimal velocity mapping than in our previous design, and an up to 5-fold improvement in the (modelled)

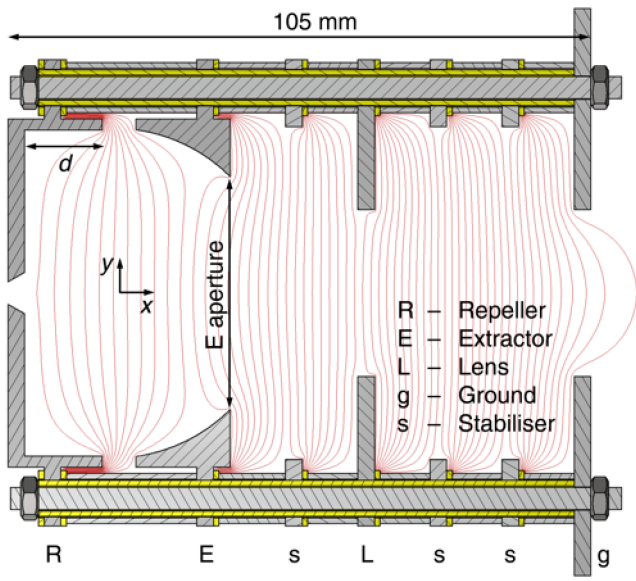

FIG. 1. Cross-sectional view of the new VMI optics, illustrating the electrode geometries and the lines of equipotential returned by the SIMION modelling. Stainless steel components and insulating components are shaded grey and yellow, respectively.

limiting velocity (i.e., $\Delta r/r$ or $\Delta v/v$) resolution. The overall assembly is longer (e.g., the distance between the plane of ionisation and the ground (G) electrode is 82 mm (cf. 70 mm in the previous design)). The electrodes and support rods are made of stainless steel, and the latter are covered with an insulating sleeve which is in turn covered with a thin stainless steel sleeve that is electrically connected to the adjacent lower potential electrode—thereby ensuring that at no stage do the ions of interest have direct line of sight to any insulating part.

There are an infinite number of possible geometry configurations that could, in principle, be modelled in the quest for optimum performance. Thus, it was necessary to adopt a systematic approach to optimising the ion optics design, within the constraints imposed by the physical size of the existing vacuum chamber, the diameter of the annular cryo-shield surrounding the interaction region, and the requirement that the laser propagation axis must lie between the repeller (R) and extractor (E) electrodes. The ion optics geometry was modified iteratively using a routine written in Lua, and a series of 2-D simulations run to determine the velocity mapping capability of each configuration. Initial simulations concentrated on understanding the effects of changing aspects of the geometry (e.g., aperture diameters and electrode spacings). These preliminary calculations encouraged more thorough investigation of three design features: (i) the shape/depth of the R electrode, (ii) the shape/curvature of the E electrode, and (iii) the extent to which the electrode assembly design shields the acceleration region from stray fields. Our exploration of each of these factors is now described. Further details, the results of supporting SIMION simulations, and illustrative test data for photolysis of IBr are included in the supplementary material.[3]

(i) Our earlier design introduced a top hat shaped R electrode in place of the traditional annular plate.[25] Such a design, in combination with a conical E electrode, yielded field lines that are suitably parallel to one another and perpendicular to the extraction axis. The present modelling reveals that further improvements in velocity mapping capability can be achieved by increasing the recess depth, d, of this R electrode further, as illustrated in Fig. 2(a). In practice, the additional depth that can be accommodated in the existing vacuum chamber is limited by the location of the laser beam axis (and the entrance and exit windows) relative to the bulkhead that supports the skimmer separating the source and interaction regions, but the simulations suggest a ~2-fold improvement in the minimum $\Delta r/r$ should be achieved (with both the previous and new ion optics designs) upon increasing d to ~14 mm.

(ii) The earlier design[25] also introduced a thicker E electrode with a conical aperture as a route to reducing chromatic and spherical aberrations and shielding the ions of interest from external stray fields. The larger volume created by using appropriately shaped R and E electrodes results in a weaker field gradient in the interaction region. This "soft focussing" configuration offers several potential benefits. The cloud of ions formed in the interaction region has more time to expand before entering the later acceleration and TOF regions—with consequent benefits for slice imaging (see the supplementary material[3]). Further, the ions and their resulting trajectories are less sensitive to their point of creation in the interaction region (cf. when using standard flat, annular electrodes). The velocity mapping condition is thus much less sensitive to small changes in laser alignment or in the electrode voltages, and the volume within which good velocity mapping can be achieved is substantially increased. Introducing a spherical/curved surface in place of the previous conical aperture further improves the field definition within the interaction volume, resulting in a ~20% improvement in $\Delta r/r$ (for the same entrance and exit aperture diameters). As Fig. 2(b) shows, this can be further improved by increasing the aperture of the E electrode which, in the new design, comprises an entrance face defined by a sphere of radius 29.1 mm (centred on the TOF axis) and entrance and exit apertures of, respectively, 56 mm (as before) and 44 mm. As noted previously,[37] use of a spherical entrance surface also ensures that the desired linear relationship between image radius (r) and ion velocity (v) extends all the way to $r = 0$.

(iii) Additional large aperture "stabilising" electrodes have been introduced between the E and L electrodes and between the L and G electrodes (all electrically linked via a resistor chain), as shown in Fig. 1. These provide further

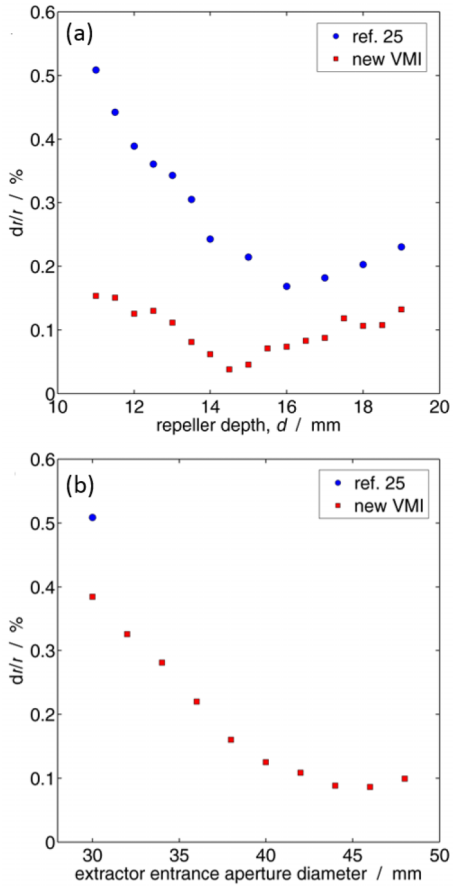

FIG. 2. Illustrations of the $\Delta r/r$ resolution returned by SIMION modelling of the new (and previous (Ref. 25)) velocity mapping ion optics for (a) different depths d of the R electrode and (b) different aperture diameters for the E electrode with a spherical entrance face. For each new geometry, the simulations employ the best operational voltages (holding V_R fixed at +2.5 kV) and assume the ejection of $^{35}Cl^+$ ions with 1.5 eV kinetic energy perpendicular to the time-of-flight axis, from a volume with $\Delta x = 0.5$ mm in the TOF direction and $\Delta y = 2$ mm in the laser propagation direction.

improvements in field definition in the later acceleration regions and provide a valuable counter against perturbing fields from the earthed support rods and any other external influences.

Further comparative simulations and sample Br and/or I atom images from the near UV photodissociation of jet-cooled IBr molecules recorded with the new ion optics assembly are included in the supplementary material.[3]

B. *Ab initio* calculations

Using the Molpro computational package,[38] the ground state minimum energy geometries of 2-iodothiophene and 2-bromothiophene were optimised using Møller-Plesset second order perturbation theory (MP2) and Dunning's contracted cc-pVDZ basis set (for the H, C, S, and Br atoms).[39] For the I atom, a pseudopotential was added to the double-ζ (cc-pVDZ-pp) basis function along with a 46 electron relativistic effective core potential.[40] Rigid body potential energy curves (PECs) were then calculated as a function of the C–X bond length, $R_{C–X}$, with the remainder of the nuclear framework fixed at the MP2 equilibrium geometry. C_s symmetry was maintained at each point along this scan. Spin orbit free (SOF) PECs were calculated using a state-averaged (SA) complete active space self-consistent field (CASSCF) reference wavefunction involving five $^1A'$, four $^1A''$, five $^3A'$, and four $^3A''$ states. The corresponding state energies were calculated using the complete active space with second order perturbation theory (CASPT2) based on the above SA-CASSCF reference wavefunction, with an imaginary level shift of 0.5 E_h to aid convergence and circumvent the effects of intruder states. The active space for these calculations comprised 12 electrons in the following nine orbitals: three occupied π orbitals, two unoccupied π^* orbitals, the p_x and p_y lone pairs centred on the X atom, and the σ and σ^* orbitals localised around the C–X bond. Spin-orbit coupled states were then calculated by evaluating the spin-orbit Hamiltonian ($\hat{H}_{SO}$) in a basis of ψ_{elec}; these states are henceforth labelled using the extended irreducible representation including both spin-orbit free and spin parts. In order to account for dynamic correlation of electrons, the obtained SOF CASPT2 energies were then used in the diagonalisation of the spin-orbit coupling matrix.

Gaussian 09[41] was used to calculate "relaxed" PECs along the C(2)–S ring opening coordinate ($R_{C–S}$). These calculations started from the MP2 optimised ground state geometry (above). $R_{C–S}$ was then extended in 0.1 Å increments to $R_{C–S}$ = 3.7 Å, and at each value, the remainder of the nuclear framework was optimised at the MP2/LANL2DZ level (with C_s symmetry constraints). The excited states were then calculated at these various relaxed ground state geometries along $R_{C–S}$ using SOF CASPT2. These CASPT2 calculations utilised the same state averaging, active space, basis set, and imaginary level shift as the previously described calculations along $R_{C–X}$.

Following C(2)–S bond extension, various ground state minima and transition state (TS) geometries linking potential isomers were calculated using Density Functional Theory (DFT) along with the Becke 3-parameter Lee-Yang-Parr (B3LYP) functional. The default 6-311G(*d*,*p*) basis set embedded within Gaussian 09 was used for the 2-bromothiophene calculations, whereas for 2-iodothiophene, the functions of the equivalent 6-311G(*d*,*p*) basis set were generated artificially (and are listed in the supplementary material[3]). The biradicals formed upon ring-opening in 2-bromo- and 2-iodothiophene were identified as local minima and could thus be optimised in the normal way using DFT/B3LYP/6-311G(*d*,*p*) and a singlet spin multiplicity. Given the evident differences in the Br product recoil velocity distributions from 267 nm photolysis of 2- and 3-bromothiophene,[9] we also attempted to characterise the equivalent ring-opened biradical on the ground state PES of 3-bromothiophene. These calculations were unsuccessful—minimising instead to a lower energy cyclopropene adduct. Thus, the lowest root of triplet spin multiplicity was used to optimise this critical point in the case of 3-bromothiophene, and a linear interpolation in internal coordinate (LIIC) was then scanned (using the above level of DFT) between the ring opened biradical and the cyclopropene adduct in order to establish the energy profile along this coordinate.

III. RESULTS AND DISCUSSION

Near UV absorption spectra of the two title halothiophenes are shown in Figure 3, along with an illustrative molecular structure. Both spectra show an intense band centred at ~230-240 nm and a tail stretching to longer wavelengths that is much more evident in the case of 2-iodothiophene. The 2-iodothiophene absorption profile agrees well with that reported previously (in cyclohexane solution)[10] but, additionally, shows a sequence of diffuse resonances separated by ~630 cm^{-1} on the long wavelength side of the intense feature. Analogy with bare thiophene (and the present *ab initio* calculations, *vide infra*) suggests that this feature is associated with one or more $\pi^* \leftarrow \pi$ excitations and that these resonances are likely attributable to symmetric (or antisymmetric) C–S–C stretch motions. The long wavelength tail can be viewed as the analogue of the $\sigma^* \leftarrow n/\pi$ "A-band" absorptions of other alkyl (and aryl) halides. The greater prominence and extent of this tail in the spectrum of 2-iodothiophene accords with the findings of our recent studies of 4-bromo- and 4-iodophenol;

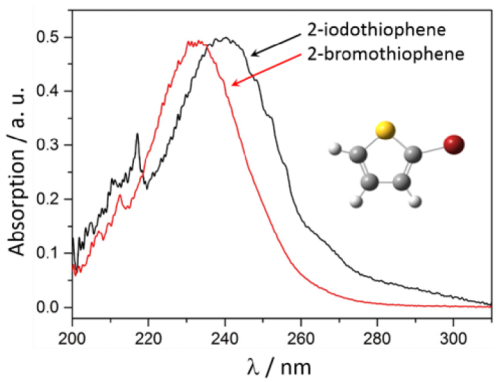

FIG. 3. Room temperature near-UV absorption spectra of 2-bromo- and 2-iodothiophene recorded using the vapour above a small sample of the neat liquid in an atmosphere of air.

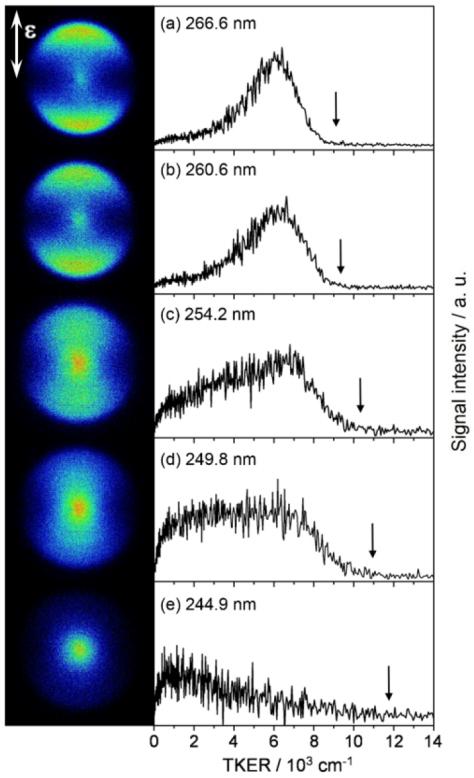

FIG. 4. Images of $Br(^2P_{3/2})$ products resulting from photolysis of jet-cooled 2-bromothiophene at λ = (a) 266.6 nm, (b) 260.6 nm, (c) 254.2 nm, (d) 249.8 nm, and (e) 244.9 nm, with the **ε** vector of the photolysis laser radiation aligned vertically in the plane of the images (as shown in panel (a)). The TKER spectrum derived from analysis of each data set is shown to the right of each image, with the vertical arrow showing the $TKER_{max}$ value assuming $D_0(R-Br) = 29\,000\ cm^{-1}$.

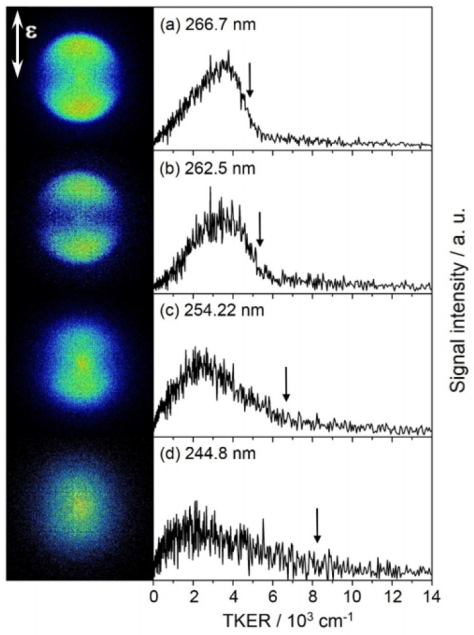

FIG. 5. Images of $Br(^2P_{1/2})$ products resulting from photolysis of jet-cooled 2-bromothiophene at λ = (a) 266.7 nm, (b) 262.5 nm, (c) 254.2 nm, and (d) 244.8 nm, with the **ε** vector of the photolysis laser radiation aligned vertically in the plane of the images (as shown in panel (a)). The TKER spectrum derived from analysis of each image is shown on the right, with the vertical arrow indicating the $TKER_{max}$ value assuming $D_0(R-Br) = 29\,000\ cm^{-1}$.

nominally spin-forbidden singlet-triplet transitions appear with much greater transition strength in the latter.[8]

A. Ion imaging data

The left hand panels in Figs. 4–7 show raw images of, respectively, the Br and Br* fragments resulting from photolysis of 2-bromothiophene and the I and I* fragments from photolysis of 2-iodothiophene, recorded at several different near UV wavelengths. For consistency, only pancaked images are reported in the main paper. All images of a given species were recorded using the same extraction voltages (i.e., the respective radii are reliable indicators of the relative velocity), and in all cases, the electric (**ε**) vector of the photolysis laser radiation was vertical (i.e., parallel to the front face of the detector) as shown on the first image in each figure. The corresponding total kinetic energy release (TKER) spectra (shown to the right of each image) were derived using the appropriate Jacobian together with the assumption that the unobserved fragment partnering the Br/I atom has chemical formula C_4SH_3 and mass m = 83.13 u.

These data show a number of trends, which we review by first focussing on 2-bromothiophene. The Br image recorded at longest photolysis wavelength—a one colour experiment at 266.6 nm—shows a fast, anisotropic recoil velocity distribution, peaking at TKER ~6000 cm^{-1}, with a full width half maximum (FWHM) of ~3000 cm^{-1}, and an associated anisotropy parameter β ~ 2, i.e., the limiting value for prompt axial recoil following excitation via a transition dipole moment (TDM) for which is aligned parallel to the breaking bond—as reported (following photolysis at 267 nm) by Zhang *et al.*[9] Moving to shorter wavelengths, the anisotropic fast ring fades in relative intensity and is progressively replaced by a smaller, isotropic feature—exemplified by the data recorded at 244.9 nm (Fig. 4(e)). The TKER spectrum derived from this image peaks close to zero.

The Br* fragment images from photolysis of 2-bromothiophene (and the TKER spectra derived from them) reveal a similar trend. The images recorded at longer wavelengths, i.e. at 266.7 and 262.5 nm (Figs. 5(a) and 5(b)), are dominated by an anisotropic feature, peaking at TKER ~3500 cm^{-1}, with a FWHM of ~3000 cm^{-1}. The β parameter is velocity dependent: ~1.5 around the peak of the distribution and declining at lower TKER. The weak Br* image taken at λ = 244.8 nm, in contrast, is essentially isotropic and peaks at low TKER.

I and I* images from 2-iodothiophene were recorded over a greater range of photolysis wavelengths and again show similar trends. A weak one-colour I atom signal was discernible following excitation at 303.68 nm. As Fig. 6(a) shows, these I atoms display a narrow (~2000 cm^{-1} (FWHM)), anisotropic (β ~ 1.7) translational energy distribution peaking at TKER ~7000 cm^{-1}, which initially expands upon scanning to shorter wavelengths, but then shrinks (in radius), becomes more isotropic, fades (in relative intensity), and is supplemented by a slower, isotropic component as the photolysis wavelength is reduced. Nonetheless, as Fig. 6(f) shows, a

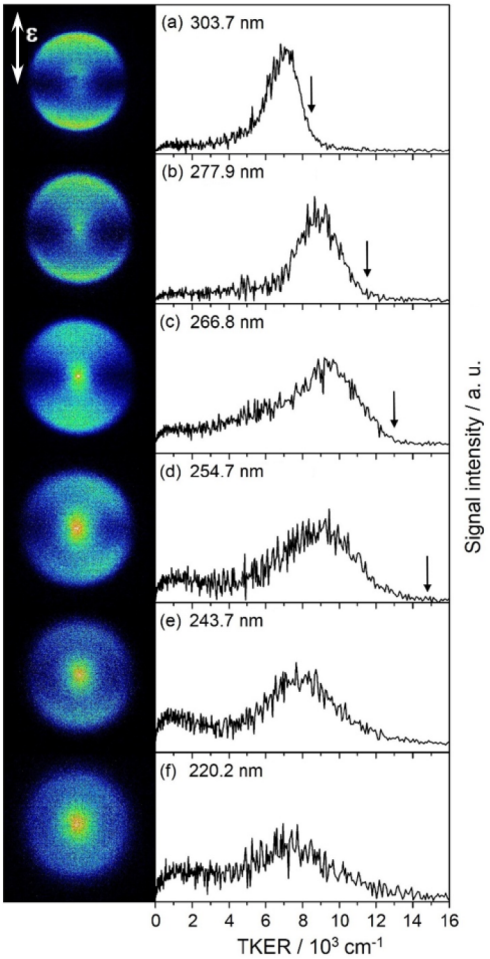

FIG. 6. Images of $I(^2P_{3/2})$ products resulting from photolysis of jet-cooled 2-iodothiophene at λ = (a) 303.7 nm, (b) 277.9 nm, (c) 266.8 nm, (d) 254.7 nm, (e) 243.7 nm, and (f) 220.2 nm, with the **ε** vector of the photolysis laser radiation aligned vertically in the plane of the images (as shown in panel (a)). The TKER spectrum derived from analysis of each data set is shown on the right, with the vertical arrow showing the $TKER_{max}$ value assuming $D_0(R-I) = 24\,500\ cm^{-1}$.

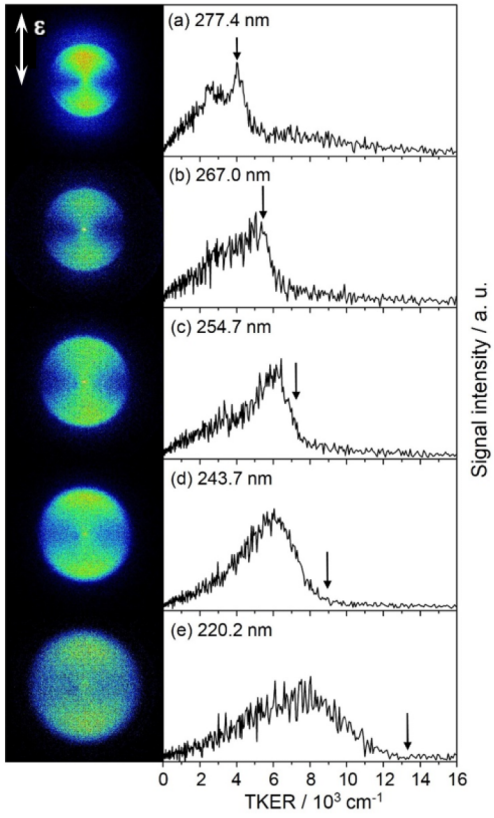

FIG. 7. Images of $I(^2P_{1/2})$ products resulting from photolysis of jet-cooled 2-iodothiophene at λ = (a) 277.4 nm, (b) 267.0 nm, (c) 254.7 nm, (d) 243.7 nm, and (e) 220.2 nm, with the **ε** vector of the photolysis laser radiation aligned vertically in the plane of the images (as shown in panel (a)). The TKER spectrum derived from analysis of each data set is shown on the right, with the vertical arrow showing the $TKER_{max}$ value assuming $D_0(R-I) = 24\,500\ cm^{-1}$.

faster (albeit more anisotropic) component peaking at TKER ~7000 cm^{-1} is still discernible at λ = 220.2 nm.

As in the cases of iodobenzene,[6] various fluorinated iodobenzenes,[7] and 4-iodophenol,[8] the I^* images measured following excitation of 2-iodothiophene at long wavelength show hints of product vibrational structure, as illustrated in Fig. 7(a) (λ = 277.4 nm). Following past precedent, we assign the most obvious peak in the TKER spectrum taken at longest wavelength (indicated by the arrow in Fig. 7(a)) to formation of I^* atoms together with radical fragments in their ground (i.e., zero-point, v = 0) vibrational level. Such an attribution allows estimation of the C–I bond strength via the usual energy conservation relationship,

$$D_0(R-I) = E_{phot} - A(I) - TKER_{max},$$

where R represents the (α-)thienyl (sometimes also referred to as the thiophenyl) radical, E_{phot} is the photolysis photon energy, $A(I)$ is the spin-orbit energy of the I^* atom (7603 cm^{-1}), $TKER_{max}$ is the TKER associated with this fastest feature, and we neglect the small amount of internal excitation in the jet-cooled parent molecules; this analysis yields $D_0(R-I) = 24\,500 \pm 500\ cm^{-1}$—a value that is sensibly consistent with a typical C–I bond strength in other aromatic systems.[6–8] *Ab initio* calculations for the ground state thienyl radical provide clues as to the assignment of the vibrational peak observed in Fig. 7(a). A unique assignment is not possible given the limited energy resolution, but the observed wavenumber separation (~1500 cm^{-1} from the peak assigned to v = 0 products) is sensibly consistent with one quantum of the in-plane symmetric (and antisymmetric) C–C stretching modes—see the supplementary material.[3] We note that the former is prominent in the previously reported RR spectra of 2-iodothiophene (albeit when exciting at slightly shorter wavelengths).[10]

The short vertical arrows at the high TKER end of the spectra shown in Figs. 6 and 7 indicate the maximum TKERs predicted for the I (or I^*) + R products arising at each photolysis wavelength given $D_0(R-I) = 24\,500\ cm^{-1}$. These data emphasise that the mean TKER, ⟨TKER⟩, associated with each channel is rather insensitive to changes in E_{phot}, implying progressively greater partitioning of the available energy (i.e., of $E_{phot} - D_0(R-I)$) into internal excitation of the thienyl radical product—a conclusion that, again, is in good accord with those reached from the earlier resonance Raman studies.[10]

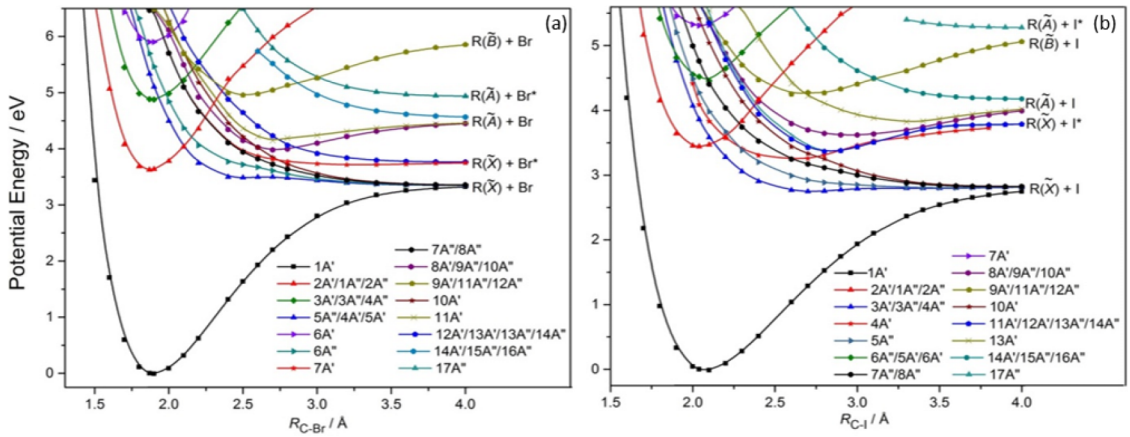

FIG. 8. Diabatic, SO resolved PECs along R_{C-X} for the ground and lower lying excited states of (a) 2-bromothiophene and (b) 2-iodothiophene.

None of the TKER distributions derived from the Br or Br* images from photolysis of 2-bromothiophene show any hints of product vibrational structure (as was the case, also, in the imaging study of 4-bromophenol photolysis[8]). Nonetheless, if we assume similar dissociation dynamics to that revealed by 2-iodothiophene and that the $TKER_{max}$ value for products formed from 2-bromothiophene photolysis at the longest UV wavelengths similarly lies on the fast edge of the high TKER feature (as shown by the short vertical arrow in both Figs. 4(a) and 5(a)), we arrive at a C–Br bond strength D_0 (R – Br) ~ 29 000 cm^{-1} (given A(Br) = 3685 cm^{-1}) that is again sensibly consistent with values reported for bromobenzene (342.8 kJ mol^{-1}, 28 650 cm^{-1}, Ref. 42) and for 4-bromophenol (28 700 cm^{-1}, Ref. 8), but substantially larger than an earlier suggested C–Br bond strength in 2-bromothiophene.[43] As the other panels in Figs. 4 and 5 show, tuning to shorter photolysis wavelengths again results in a relative increase in the internal energy partitioned into the thienyl partner.

B. *Ab initio* calculations of C–Br/C–I bond fission and C–S ring opening pathways in 2-bromothiophene and 2-iodothiophene

Figures 8(a) and 8(b) present SO resolved PECs along R_{C-X} for the ground and lower energy excited states of, respectively, 2-bromothiophene and 2-iodothiophene. In both cases, the molecule has been constrained to planar geometries, and the PECs have been approximately "diabatised" in terms of $(n/\pi)\sigma^*$ and $\pi\pi^*$ states by inspecting the energies, symmetries, and wavefunction coefficients. The adiabatic SO resolved potentials from which these are derived are shown in the supplementary material.[3] As in the case of the iodobenzenes[6,7] and halophenols,[8] the lowest repulsive potentials all arise from $\sigma_{C-X}^* \leftarrow n/\pi$ excitations; these potentials correlate with the ground ($\tilde{X}^2A'$) state thienyl + X/X* dissociation limits. The spin-orbit split analogues involving the first ($\tilde{A}^2A''$) excited state of the thienyl radical lie higher in energy, while the (diabatically) bound interloper PECs arise from excitations to ring centred π^* orbitals. The calculated vertical excitation energies suggest that many of these excited states could be sampled within the wavelength ranges explored in the present study, but analogy with the previous VMI studies of the X/X* products from photolysis of iodobenzenes and 4-iodo- and 4-bromophenol suggests that the $\sigma^* \leftarrow n/\pi$ TDMs returned by the present calculations are likely to be of limited value in deciding which are the optically "bright" states (illustrative TDMs are listed in the supplementary material[3]). Rather, as in those cases,[6–8] the observation that the faster X and X* products formed at long excitation wavelengths show near limiting parallel recoil anisotropy suggests that the populated states are those that gain intensity by vibronic interaction with the higher lying, intense, C–X bond centred, $\sigma^* \leftarrow \sigma$ transition.

The predicted energy separations between the various asymptotic limits merit comment. The present calculations reproduce the Br/Br* and I/I* spin-orbit splittings well but predict a larger separation between the $\tilde{A}$ and $\tilde{X}$ states of the thienyl radical (~1.25 eV) than that derived from photodetachment studies of the thiophenide anion (~0.6 eV, Ref. 44). This is not surprising, given that the PECs are derived via rigid body scans and thus preclude any structural relaxation of the ring. Nonetheless, the present calculations confirm the earlier suggestion that $(n/\pi)\sigma^*$ excited states (i.e., states that are dissociative with respect to C–X bond extension, and which correlate to X or X* products) are dominant contributors to the long wavelength tail of the respective absorption spectra and locate the minimum of the first (spin-allowed) $\pi^* \leftarrow \pi$ transition at ~5.3 eV (~5.9 eV) for X = I (Br), in reasonable accord with the observed absorption maxima (Fig. 3).

Cuts through the first few SOF potentials of 2-bromothiophene and 2-iodothiophene along the R_{C-S} stretch (ring-opening) coordinate are shown in Figs. 9(a) and 9(c), respectively. The corresponding adiabatic SOF PECs along R_{C-X} are shown alongside, in Figs. 9(b) and 9(d). The S_0 state is stable with respect to ring opening in both halothiophenes, and its PEC thus rises steadily with increasing R_{C-S}. In contrast, the PECs for the $1^1A''$ and $2^1A''$ states (and for their triplet analogues, all of which arise via $\sigma_{C-S}^* \leftarrow (n/\pi)$ excitations) show obvious instability with respect to extending R_{C-S}. Notwithstanding the limitations of these SOF PECs (all of which are calculated at the MP2 relaxed ground state geometries), they clearly point to the availability of exoergic pathways from the bright $^1\pi\pi^*$ ($2^1A'$) state, via one or more $(n/\pi)\sigma_{C-S}^*$ PECs, to extended C–S bond lengths and regions of conical intersection with the S_0 state potential.

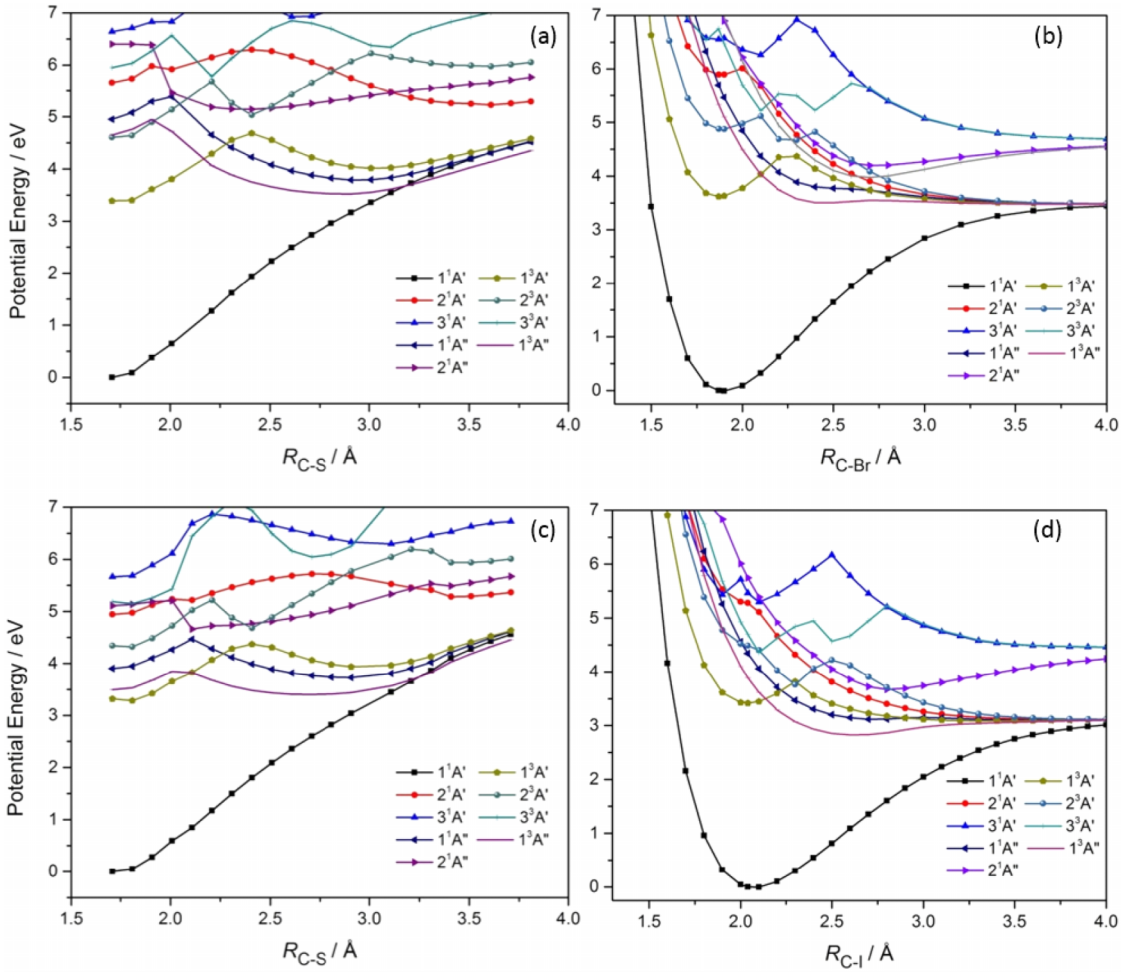

FIG. 9. Approximately diabatised SO free PECs along the $R_{C–S}$ (ring-opening) coordinate and $R_{C–X}$ stretch for the first few singlet (solid lines) and triplet (dashed lines) states of 2-bromothiophene ((a) and (b), respectively) and 2-iodothiophene ((c) and (d), respectively).

Figure 10 summarises some of the various possible fates of 2-halothiophene molecules following non-adiabatic transfer to the S_0 PES. The primary ring-opened structure is a biradical (structure **B**) that can exist as essentially degenerate *cis* and *trans* isomers—both of which are unstable with respect to the original ground state halothiophene. **B** can also isomerise to various ring-opened isomers (including structures **D**-**G**) via transition states, three of which that involve migrating (at most) one atom from the biradical structure (**TS1**, **TS2**, and **TS3**) have been optimised. As Fig. 10 also shows, a range of Br + radical (**H**, **I**, **J**, **K**, as well as **R**) dissociation limits are calculated to lie below the energy of a 250 nm photon (illustrated by the horizontal red line). The various structures and product pairs, along with their energies (in cm^{-1}, defined relative to that of the ground state minimum), are detailed below the figure, along with the corresponding quantities for 2-iodothiophene (in parentheses). The calculated R–Br and R–I bond strengths are seen to match well with the experimental values derived in Sec. III A. Readers should also note that the dashed lines at the far right of Fig. 10 are simply intended to correlate various isomers to particular dissociation products; we have not checked for the presence (or otherwise) of any barrier in the various fragmentation paths.

C. A plausible explanation for the observed wavelength dependent fragmentation dynamics

The X and X* images measured at the longer UV wavelengths are very reminiscent of those reported previously following photolysis of, for example, iodobenzenes[6,7] and 4-iodo- and 4-bromophenol.[8] The X and X* products recoil with close to the maximum speed permitted by energy conservation and with close to limiting parallel anisotropy. The velocities of the faster X/X* products increase little upon tuning to shorter excitation wavelengths, implying a preferential partitioning of the additional photon energy into internal (vibrational) excitation of the thienyl radical partner. As in the previously studied aryl iodides and bromides, such behaviour is fully consistent with population of one or more $(n/\pi)\sigma^*$ excited states and prompt C–X bond fission. The progressive increase in product vibrational excitation can be understood on Franck-Condon grounds, given the changes in equilibrium ring geometry upon $\sigma^* \leftarrow (n/\pi)$ excitation and subsequent evolution to the radical product. As noted above, the near limiting parallel recoil anisotropy of the X and X* products can be understood if (as has been shown in detail in the case of methyl iodide[45]) the participating $(n/\pi)\sigma^*$ state(s) gains transition probability by vibronic interaction with a

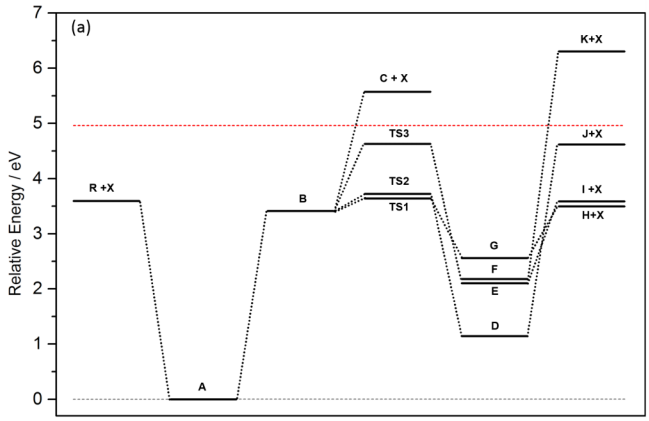

(b) Structure	Energy/cm^{-1}	Structure	Energy/cm^{-1}
A	0	D	9230 (9490)
R+X	28480 (24650)	E	16950 (16520)
B (trans)	27530 (27560)	F	17570 (16850)
B (cis)	27530 (27820)	G	20680 (20360)
C (trans) +X	44930 (41100)	H+X	28220 (24390)
C (cis) +X	45400 (41560)	I+X	28920 (25090)
TS1	29530 (28920)	J+X	37240 (33410)
TS2	30020 (29810)	K+X	50840 (47010)
TS3	37330 (36520)	--	--

FIG. 10. Diagram showing the calculated relative energies of 2-bromothiophene (**A**), the biradical intermediate **B** formed upon C–S bond fission, TSs leading to various ring-opened isomers (**D**-**G**), and selected Br + radical (**H**, **I**, **J**, **K**) product limits. The dashed lines at the far right of the figure simply correlate given structures to particular dissociation products; we have not checked for the presence (or otherwise) of any barrier in the various fragmentation paths. The various structures along with their energies (in cm^{-1}, defined relative to the ground state minimum) are detailed below, together with the corresponding quantities for 2-iodothiophene (in parentheses). The horizontal dashed line indicates the total energy reached upon absorption of a 250 nm photon.

higher lying, C–X bond localised $\sigma\sigma^*$ state, and the subsequent bond fission occurs on a time scale that is fast compared to the molecular rotational period.

The primary novelty of the present study, however, is the clear switch in energy disposal upon reducing the excitation wavelength. This switch is revealed by the appearance (and growing dominance) of a slow, isotropic component within the X and X* images—more obviously in the case of 2-bromothiophene—and roughly coincides with the start of the obvious increase in parent absorption that we associate with $\pi^* \leftarrow \pi$ absorption (Fig. 3). Careful inspection of Figs. 6 and 7 also shows that the "fast" component in the I and I* images slows and becomes less anisotropic as the photon energy is increased further.

The PES for this $\pi\pi^*$ state (the $2^1A'$ state in Fig. 9) shows CIs (at geometries not far from the vertical Franck Condon region) with other excited states, the potential energies of which decline with increases in R_{C-X} and/or R_{C-S}. Thus, it is reasonable to propose that excitation at these shorter wavelengths populates the (diabatically bound) $2^1A'$ state, which can then decay by coupling to states that are dissociative with respect to C–X and/or C–S bond extension. Which of these decay processes dominates (i.e. the C–X bond fission or the channel initiated by C–S bond extension) will be sensitively dependent upon the respective minimum energy pathways from the $2^1A'$ state, and the details of the coupling modes that facilitate the population transfer.

The almost total absence of "fast" Br/Br* products in the images recorded following photolysis of 2-bromothiophene at $\lambda \sim 245$ nm suggests that (i) the partial absorption cross section to the $2^1A'$ state far exceeds that to the underlying $(n/\pi)\sigma^*$ state(s)—consistent with the relative weakness of the long wavelength tail in the UV absorption spectrum of 2-bromothiophene—and (ii) C–S bond extension constitutes the major decay pathway from the $2^1A'$ state, and the subsequent nuclear motion samples the predicted region of CI with the S_0 PES at extended C–S bond lengths. Radiationless transfer at this CI yields highly vibrationally excited S_0 molecules. These have more than enough internal energy to decay not only by R–Br bond fission (yielding thienyl cofragments) but also to ring-open, isomerise, and decay to yield slow Br fragments in tandem with a range of C_4H_3S radical products. Figure 10 suggests similar energetics for C–Br bond fission leading to ring closed (**R**) and some of the more stable ring opened radical products (e.g., **H** and **I**). Entropic considerations might favour the latter products, but any serious discussion of the likely product yields would require better knowledge of the topology of the CI via which population is funnelled to the biradical intermediate on the S_0 PES and of the rate with which the latter can overcome the barrier to the stable ring-opened products featured on the right hand side of Fig. 10.

The data for 2-iodothiophene are less clear cut but, again, the relative yield of slow I atoms increases upon tuning to shorter wavelengths—consistent with initial excitation to the corresponding $2^1A'$ state and radiationless transfer to (and unimolecular decay from) highly vibrationally excited S_0 molecules formed by coupling through the predicted CI at extended R_{C-S}. The "fast" I/I* feature also persists at shorter wavelengths, however. This could be explained by one, or other, or both of two mechanisms. The first recognises the (relatively) greater partial absorption cross sections of the $\sigma_{C-I}^* \leftarrow n/\pi$ excitations in 2-iodothiophene (Fig. 3), while the second assumes that, following excitation to the $2^1A'$ state, the threshold energies for predissociation enabled by C–I and C–S bond extension are more similar than in 2-bromothiophene. The evident reduction in the TKER and recoil anisotropy of the "fast" I signal at shorter wavelengths hints that C–X bond fission is a relatively more important decay channel from the $2^1A'$ state of 2-iodothiophene than in the case of 2-bromothiophene.

Finally, we contrast the fast, anisotropic Br and Br* product velocity distributions formed in the 267 nm photolysis

of 2-bromothiophene with the slow, isotropic distributions observed when exciting 3-bromothiophene at this same wavelength.[9] The latter are reminiscent of that found when exciting 2-bromothiophene at much shorter wavelengths (below ~245 nm). As noted previously, all of our attempts to characterise the analogue of biradical **B** on the S_0 PES of 3-bromothiophene minimised to a lower energy cyclopropene adduct (an enantiomer of **G**), which will have ample internal energy to decay further (e.g., to **H** + X products). The published photolysis data for 3-bromothiophene may thus be explicable if the corresponding $\sigma_{C-S}^* \leftarrow (n/\pi)$ PESs are somewhat red-shifted, cf. 2-bromothiophene, and provide an efficient route for funnelling photoexcited molecules to regions of CI with the S_0 PES and thence to C–Br bond fission on this latter PES. Photolysis studies of 3-halothiophenes at a range of (longer) UV excitation wavelengths could be useful in confirming (or refuting) this proposal.

IV. CONCLUSIONS

The near UV photofragmentation dynamics of jet-cooled, gas phase 2-bromo- and 2-iodothiophene molecules have been investigated at many different excitation wavelengths by measuring the velocity distributions of the X/X* products using a VMI spectrometer equipped with a new, purpose designed ion optics assembly. The new ion optics design is not much more complicated than the traditional flat, annular electrode stack and offers a number of potentially significant advantages: stable velocity mapping from a larger interaction volume, protection from stray fields, improved limiting velocity resolution, and natural compatibility with slice imaging. The present study addressing the photodissociation of a 9-atomic system does not provide an appropriate vehicle for illustrating the predicted velocity resolution. As discussed in the supplementary material,[3] the ultimate test of the resolving power of the new ion optics assembly should involve photodissociation studies of fully quantum state selected parent molecules, such as those reported by the Janssen group for methyl iodide.[46]

The present imaging study reveals a marked change in photofragmentation behaviour upon tuning to shorter excitation wavelengths, particularly in the case of 2-bromothiophene. Long wavelength excitation results in prompt C–X bond fission; the resulting X/X* products are formed with kinetic energies close to the maximum allowed by energy conservation and with near limiting parallel recoil anisotropy. Companion *ab initio* calculations show that these products arise following excitation to one or more $(n/\pi)\sigma^*$ states and serve to highlight the photophysical similarities with other aryl iodides (and bromides) when excited at longer UV wavelengths.[4–8]

At shorter wavelengths, the anisotropic fast ring associated with these products fades in relative intensity and is progressively replaced by a smaller, isotropic feature that signifies the formation of much slower X/X* atom products. The appearance of this new channel roughly coincides with the onset of more intense parent absorption to the $2^1A'$ excited state. *Ab initio* theory suggests that this $\pi\pi^*$ excited state can predissociate by interaction with neighbouring $(n/\pi)\sigma^*$ states, the potentials for which decline in energy along both the R_{C-X} and R_{C-S} stretch coordinates. The 2-bromothiophene data can be understood if the latter offers the lower energy decay route from the optically bright $2^1A'$ state, to a CI with the ground state PES at extended C–S bond lengths. The present DFT/B3LYP/6-311G(d,p) calculations suggest that the resulting biradicals have more than sufficient energy to sample the configuration space associated with several different isomeric forms of the starting molecule and to form both ring closed and ring opened C_4H_3S radical products following subsequent C–Br bond fission on the S_0 PES.

The data for 2-iodothiophene are less clear cut but, again, the relative yield of slow I atoms increases markedly upon tuning to shorter wavelengths—consistent with initial excitation to the corresponding $2^1A'$ state and radiationless transfer to (and unimolecular decay from) highly vibrationally excited S_0 molecules formed by coupling through the predicted CI at extended R_{C-S}. The "fast" I/I* feature also persists at shorter wavelengths, however. This could be explained by one, or other, or both of two mechanisms. The first recognises the (relatively) greater partial absorption cross sections of the $\sigma_{C-I}^* \leftarrow n/\pi$ excitations in 2-iodothiophene, while the second assumes that following excitation to the $2^1A'$ state, the thresholds for predissociation enabled by C–I and C–S bond extension are closer in energy than in 2-bromothiophene.

It is interesting to compare the present findings with those from recent condensed phase studies of thiophenone in acetonitrile solution, wherein the photoexcited parent molecules were similarly deduced to convert to highly vibrationally excited levels of the ground (S_0) state by coupling via a CI at extended C–S bond lengths[19] Ring opening was confirmed in that case by the observation of ketene products, but the time evolution of the parent bleach signals indicated that the majority (~60%) of these highly vibrationally excited S_0 molecules relax and re-thermalise as the ring closed thiophenone. Such vibrational relaxation is not available in the present isolated molecule gas phase studies, so eventual dissociation is assured on energetic grounds, but the relative probabilities for forming ring opened or ring closed fragmentation products remains an open question.

ACKNOWLEDGMENTS

The authors are grateful to EPSRC (Programme Grant Nos. EP/G00224X and EP/L005913), to the TSB (Knowledge Transfer Partnership KTP008481 that stimulated the Bristol-Photek collaboration), to the Marie Curie Initial Training Network ICONIC (Contract Agreement No. 238671), and to Rebecca Ingle, Keith Rosser, Dr. Stuart Greaves, Dr. James Smith, Dr. Andreas Wenge, Dr. Eckart Wrede, and Dr. Dimitrios Zaouris for their many and varied contributions to this work. Data accessibility: The underlying data for this paper has been placed in the University of Bristol's research data repository and can be accessed using the following DOI: 10.5523/bris.qwlb0o0e9tbd1bqojd8gxrnjj.

[1]A. L. Sobolewski, W. Domcke, C. Dedonder-Lardeux, and C. Jouvet, Phys. Chem. Chem. Phys. **4**, 1093 (2002).
[2]M. N. R. Ashfold, G. A. King, D. Murdock, M. G. D. Nix, T. A. A. Oliver, and A. G. Sage, Phys. Chem. Chem. Phys. **12**, 1218 (2010).

[3]See supplementary material at http://dx.doi.org/10.1063/1.4921315 for additional details regarding the design and implementation of the new ion optics assembly, the 6–311G(*d*,*p*) basis set used for the 2-iodothiophene calculations, adiabatic SO resolved potentials along R_{C-X} for 2-bromo- and 2-iodothiophene and calculated TDMs, and vibrational wavenumbers for the ground states of 2-bromo- and 2-iodothiophene and the thienyl radical.
[4]K. L. Han and G. Z. He, J. Photochem. Photobiol., C **8**, 55 (2007).
[5]X.-P. Zhang, Z.-R. Wei, Y. Tang, T.-J. Chao, B. Zhang, and K.-C. Lin, ChemPhysChem **9**, 1130 (2008).
[6]A. G. Sage, T. A. A. Oliver, D. Murdock, M. D. Crow, G. A. D. Ritchie, J. N. Harvey, and M. N. R. Ashfold, Phys. Chem. Chem. Phys. **13**, 8075 (2011).
[7]D. Murdock, M. B. Crow, G. A. D. Ritchie, and M. N. R. Ashfold, J. Chem. Phys. **136**, 124313 (2012).
[8]A. G. Sage, T. A. A. Oliver, G. A. King, D. Murdock, J. N. Harvey, and M. N. R. Ashfold, J. Chem. Phys. **138**, 164318 (2013).
[9]F. Zhang, Z. Cao, X. Qin, Y. Liu, Y. Wang, and B. Zhang, Acta Phys.-Chim. Sin. **24**, 1335 (2008).
[10]H.-L. Zhu, J. Liu, X. M. Zheng, and D. L. Phillips, J. Chem. Phys. **125**, 054510 (2006).
[11]X.-F. Wu, X. M. Zheng, H.-G. Wang, Y. Y. Zhao, X. G. Guan, D. L. Phillips, X. Chen, and W. H. Fang, J. Chem. Phys. **133**, 134507 (2010).
[12]H. A. Wiebe and J. Heicklen, Can. J. Chem. **47**, 2965 (1969).
[13]C.-W. Hsu, C.-L. Liao, Z.-X. Ma, and C. Y. Ng, J. Phys. Chem. **99**, 1760 (1995).
[14]F. Qi, O. Sorkhabi, A. H. Rizvi, and A. G. Suits, J. Phys. Chem. A **103**, 8351 (1999).
[15]S. Salzmann, M. Kleinschmidt, J. Tatchen, R. Weinkauf, and C. M. Marian, Phys. Chem. Chem. Phys. **10**, 380 (2008).
[16]N. Gavrilov, S. Salzmann, and C. M. Marian, Chem. Phys. **349**, 269 (2008).
[17]G. Cui and W. Fang, J. Phys. Chem. A **115**, 11544 (2011).
[18]M. Stenrup, Chem. Phys. **397**, 18 (2012).
[19]D. Murdock, S. J. Harris, J. Luke, M. P. Grubb, A. J. Orr-Ewing, and M. N. R. Ashfold, Phys. Chem. Chem. Phys. **16**, 21271 (2014).
[20]M. Stenrup and Å. Larson, Chem. Phys. **379**, 6 (2011).
[21]E. V. Gromov, C. Léveque, F. Gatti, I. Burghardt, and H. Köppel, J. Chem. Phys. **135**, 164305 (2011).
[22]C. M. Krauter, J. Möhring, T. Buckup, M. Pernpointner, and M. Motzkus, Phys. Chem. Chem. Phys. **15**, 17846 (2013).
[23]S. Prager, I. Burghardt, and A. Dreuw, J. Phys. Chem. A **118**, 1339 (2014), and references therein.
[24]D. Tuna, A. L. Sobolewski, and W. Domcke, Phys. Chem. Chem. Phys. **16**, 38 (2014).
[25]E. Wrede, S. Laubach, S. Schulenburg, A. Brown, E. R. Wouters, A. J. Orr-Ewing, and M. N. R. Ashfold, J. Chem. Phys. **114**, 2629 (2001).
[26]S. Arepalli, N. Presser, D. Robie, and R. J. Gordon, Chem. Phys. Lett. **117**, 64 (1985).
[27]A. Gedanken, M. B. Robin, and Y. Yafet, J. Chem. Phys. **76**, 4798 (1982).
[28]A. M. Wenge, T. N. V. Karsili, J. R. Diaz, M. I. Cotterell, B. Marchetti, R. N. Dixon, and M. N. R. Ashfold, "Tuning photochemistry: Substituent effects on πσ* state mediated bond fission in thioanisoles," Phys. Chem. Chem. Phys. (to be published).
[29]See http://simion.com/ for calculating electric fields and the trajectories of charged particles in those fields.
[30]T. J. Obernhuber, U. Kensy, and B. Dick, Phys. Chem. Chem. Phys. **5**, 2799 (2003).
[31]V. Dribinski, A. B. Potter, I. Federov, and H. Reisler, Chem. Phys. Lett. **385**, 233 (2004).
[32]T. Nishide and T. Suzuki, J. Phys. Chem. A **108**, 7863 (2004).
[33]J. G. Izquierdo, G. A. Amaral, F. Ausfelder, F. J. Aoiz, and L. Banares, ChemPhysChem **7**, 1682 (2006).
[34]I. Wilkinson and B. J. Whitaker, J. Chem. Phys. **129**, 154312 (2008).
[35]W. S. Hopkins, S. M. Hamilton, P. D. McNaughten, and S. R. Mackenzie, Chem. Phys. Lett. **483**, 10 (2009).
[36]R. A. Livingstone, J. O. F. Thompson, M. Illina, R. J. Donaldson, B. J. Sussman, M. J. Paterson, and D. Townsend, J. Chem. Phys. **137**, 184304 (2012).
[37]A. M. Wenge, A. Schmaunz, U. Kensy, and B. Dick, Phys. Chem. Chem. Phys. **14**, 7076 (2012).
[38]H.-J. Werner, P. J. Knowles, G. Knizia, F. R. Manby, M. Schütz *et al.*, MOLPRO, version 2010.1, a package of *ab initio* programs, University of Cardiff, Cardiff, UK, 2010, see http://www.molpro.net.
[39]T. H. Dunning, Jr., J. Chem. Phys. **90**, 1007 (1989).
[40]K. A. Peterson, B. C. Shepler, D. Figgen, and H. Stoll, J. Phys. Chem. A **110**, 13877 (2006).
[41]M. J. Frisch, G. W. Trucks, H. B. Schlegel *et al.*, GAUSSIAN 09, Revision D.01, Gaussian, Inc., Wallingford, CT, 2013.
[42]H. Zhang, R.-S. Zhang, G.-J. Wang, K.-L. Han, G.-Z. He, and N.-Q. Lou, J. Chem. Phys. **110**, 2922 (1999).
[43]C. Párkányi, Pure Appl. Chem. **55**, 331 (1983).
[44]L. M. Culberson and A. Sanov, J. Chem. Phys. **134**, 204306 (2011).
[45]A. B. Alekseyev, H.-P. Liebermann, and R. J. Buenker, J. Chem. Phys. **126**, 234102 (2007).
[46]L. Lipciuc, J. B. Buijs, and M. H. M. Janssen, Phys. Chem. Chem. Phys. **8**, 219 (2006).